INSTITUTE OF PHYSICS PUBLISHING JOURNAL OF PHYSICS: CONDENSED MATTER

J. Phys.: Condens. Matter **13** (2001) 3491–3509 www.iop.org/Journals/cm PII: S0953-8984(01)19553-6

Impact of disorder on optical phonons confined in CdS nano-crystallites embedded in a SiO_2 matrix

M I Vasilevskiy[1,4], A G Rolo[1], M J M Gomes[1], O V Vikhrova[2] and C Ricolleau[3]

[1] Departamento de Fisica, Universidade do Minho, Campus de Gualtar, 4710-057 Braga, Portugal
[2] Faculty of Physics, Nizhni Novgorod University, Nizhni Novgorod, 603600 Russia
[3] Laboratory of Minerology and Crystalography, University Paris VI and VII, 75252 Paris Cedex 05, France

E-mail: mikhail@fisica.uminho.pt

Received 29 November 2000, in final form 23 January 2001

Abstract

Non-resonant Raman spectroscopy studies of a set of CdS films annealed at different temperatures were performed and showed a direct correlation between the width of the Raman peak produced by CdS-like optical phonons and the crystalline quality of the semiconductor phase probed by x-ray diffraction (XRD) and transmission electron microscopy (TEM). In order to decribe the Raman lineshape a model proposed by Trallero-Giner *et al* (1998 *Phys. Rev.* B **57** 4664) was used, which considers optical phonons confined in small semiconductor spheres with a size distribution. The model is shown to give a good reproduction of the spectra of samples where the semiconductor phase is most crystalline. However, it required too large values of phonon damping to fit the spectra of several other samples, which, according to XRD and TEM data, do contain CdS nano-crystallites. This large broadening of the Raman peak was considered as inhomogeneous, i.e. associated with disorder. Numerical lattice dynamics calculations were performed for 2D binary clusters of arbitrary shape and three kinds of disorder were considered, (i) random variation of the Cd–S bond frequency from one nano-crystallite to another, (ii) cluster shape irregularities and (iii) fluctuations of the nearest-neighbour interaction constant within one cluster. It is shown that 'ensemble disorder' (i) can be responsible for a shoulder above the bulk CdS phonon frequency observed for some of our samples. The effect of shape disorder (ii) is similar to that of the size dispersion producing some inhomogeneous broadening of the peak. In addition, it gives rise to an extra low-frequency mode originating from the top of the acoustic band. The force constant's disorder (iii) is shown to result in a stronger asymmetric broadening of the Raman peak.

[4] Also at the Institute for Physics of Microstructures, RAS, 603600 Nizhni Novgorod, Russia.

1. Introduction

Dielectrics containing nano-scale crystalline semiconductor particles (quantum dots, QD) are interesting because of their optical properties related to the quantum confinement of electrons. The crystalline quality and the interface structure are of crucial importance for exploiting these properties [2].

The vibrational modes confined in QDs are a fascinating subject of study because they affect the electronic properties and are responsible for Raman scattering, which is one of the standard tools for the characterization of semiconductor structures. In low-dimensional semiconductors, the optical phonon modes deviate substantially from those of bulk materials. Confined phonon modes were called vibrons [1] in order to distinguish them from usual propagating phonons. The confinement effects are quite significant in very small crystals making the Raman-active vibrons sensitive to the QD size and shape. Although Raman scattering in semiconductor QDs has been studied by several groups (e.g. [3–8]), most of them analysed the spectra using oversimplified or even inadequate models. A continuum model of the optical phonon confinement in a spherical quantum dot was developed in [9–11], which treats properly both mechanical and electrostatic boundary conditions. It has been applied with a certain degree of success to the modelling of experimental Raman spectra in [1, 12]. However, this model, which uses bulk phonon dispersion curves is limited to QDs of some regular (in practice, spherical) shape and made of perfect bulk material. This is not the case in real nano-crystallites.

Disorder is inevitable in nano-structure materials. In addition to the factors present in bulk crystals (e.g. impurities), the nano-crystallite's spatial positions and sizes are random. The shape of interfaces, which produce quantum confinement, can also contain random irregularities. Finally, for nano-crystallites embedded in a glass matrix, there is an additional disorder related to fluctuating properties of the matrix or its inhomogeneity. However, only the influence of the QD size distribution on the optical properties of their ensembles has usually been considered. Effects of intrinsic disorder in semiconductor QDs have received almost no attention in the literature, except for a few recent papers [8, 13, 14]. The authors of [8] studied experimentally the compositional disorder effects on the Raman spectra of CdS_xSe_{1-x} nano-crystallites embedded in glass. However, quantum size effects on electron spectra and optical phonons were neglected in their considerations. In [13], a spread of electronic levels caused by fluctuations of shape and composition of QDs was discussed with respect to their photoluminescence spectra. In the work of Sirenko *et al* [14], some extra peaks observed in the Raman spectra of epitaxially grown $In_{0.5}Ga_{0.5}P$ QDs were attributed to the (alloy) disorder activated acoustic phonon modes.

In the present work, we study the effects of the QD size dispersion and imperfection of individual nano-crystallites on the Raman lineshape. As we will show, Raman scattering on optical vibrons in a QD composite enables rapid conclusions concerning the crystalline quality of the semiconductor phase. To describe the experimental Raman lineshape, we compare two models of the phonon confinement in QDs. One is mainly analytical and based on [9, 10]. It assumes perfectly crystalline spherical particles and includes the effect of the QD size distribution. Another model, which involves numerical lattice dynamics calculations, is proposed to investigate the impact of QD shape irregularities and the interatomic force constant's disorder in semiconductor nano-crystallites on the Raman lineshape. We believe it is relevant for nano-crystallites produced within a solid matrix at low temperatures where the atomic mobility can be insufficient to provide perfect crystallinity and smooth surface of the particles. To the best of our knowledge, this is the first discussion of such disorder effects on phonons confined in QDs in the literature.

Table 1. Annealing parameters for the RF-sputtering grown samples and parameters used in the spherical model calculations.

Sample	T (°C)	t (min)	Γ_{LO} (cm^{-1})	$\bar{R}$ (Å)	σR (Å)
A4-2	300	640	—	—	—
A4-6	500	240	—	—	—
A4-33	500	690	11	20	10
A4-35	600	210	6.5	30	6
A8-3/Si	900	60	6	20	2
St-35	—	—	7	21	4

The paper is organized as follows. Section 2 is devoted to the experimental part of the work. In section 3, we give theoretical backgrounds for the two models mentioned above and present some calculated results. Section 4 is devoted to discussion and conclusions.

2. Experimental details and results

We chose CdS nano-crystallites for our Raman studies. CdS-doped SiO_2 glass films were prepared by a conventional rf-magnetron co-sputtering method with subsequent annealing. Details of the growth and annealing procedure can be found in [15, 16]. The annealing parameters are given in table 1. We also studied some films fabricated by another group using the 'sol–gel' technique [17]. They were doped with CdS by exposing Cd-rich silica films in a hydrogen–sulphur atmosphere at 200 °C for 2 hours.

The x-ray photoelectron spectroscopy (XPS) and energy dispersive spectroscopy techniques were used to assess the chemical composition of the films. The atomic fractions of Cd and S in the surface region were estimated to each be in the range of 1–15%, without noticeable deviations from stoichiometry.

The crystalline quality of the semiconductor phase was controlled by recording x-ray diffractograms (XRDs) of the films in a grazing incidence geometry. Some representative XRD spectra have been previously published [16]. They indicate a zinc-blende structure of CdS nano-crystallites. Using the standard fitting procedure for the peaks, the crystallite size was evaluated from the XRD spectra. The optical absorption was also measured in order to check the presence of the electronic quantum confinement effects.

Both the XRD and absorption spectra of the films cannot be completely understood assuming only crystalline CdS QDs embedded in pure SiO_2 glass. As discussed in [18], the glass matrix seems to absorb the light in the 2.5–4 eV region. Probably this is because only some of the Cd and S atoms present in the film form crystallites, while the rest of them constitute some amorphous phase dissolved in the matrix. In the XRD spectra, although nano-crystallites are usually clearly seen as broadened peaks corresponding to the zinc-blende structure, some extra amorphous-like contribution is always present [16]. The latter manifests itself as a broad pedestal in the same range of angles.

Some of the samples were studied by transmission electron microscopy (TEM). By using high resolution transmission electron microscopy (HRTEM) it is possible to characterize the crystal/matrix interfaces and to determine the size and the shape of nano-crystallites. Our studies were performed on a Philips CM 20 electron microscope operating at 200 kV with a point to point resolution of 0.27 nm. Figure 1 shows one of the biggest nano-crystallites found for an RF-sputtering-grown sample A4-6. The diameter of CdS particles was found to be between 2 nm and 10 nm, with the mean value of about 5 nm.

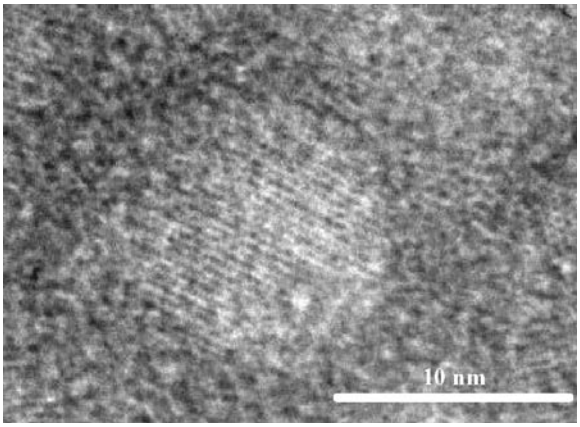

Figure 1. HRTEM micrograph of an rf-sputtering-grown CdS-doped silica film annealed at 500 °C for 4 hours. This fragment shows a 10 nm size crystallite with nearly spherical shape, although imperfections of the interface are clearly seen.

The crystalline quality of the CdS phase in rf-sputtering grown samples depends on the growth and annealing parameters, but mainly on the annealing temperature. The amorphous-like contribution dominates in films prepared at lower temperatures. The term 'crystalline quality' refers to the relative weight of the amorphous-like contribution seen in the XRD spectra compared to that of the (220), (311) and (222) peaks of the zinc-blende structure.

We studied several samples with different crystalline quality of the CdS phase. Raman spectra were measured in a backscattering geometry using various lines of an Ar^+ laser and a Jobin–Yvon T64000 triple-grating spectrometer (resolution $\sim$1 cm^{-1}).

Some of the experimental Raman spectra taken with the $\lambda = 514.5$ nm laser line are shown in figure 2. These spectra were measured at room temperature and correspond to parallel polarizations of the incident and scattered light. For perpendicular polarizations, the Raman signal was several times weaker. We did not notice any significant change in the shape of the spectra when switching the excitation wavelength to $\lambda = 488$ nm. Both these observations correspond to the non-resonant excitation conditions in our experiments. Of course, nano-crystallites of some particular size (larger than the average one) were excited resonantly in our experiments. However, the excitonic level spacing in such large QDs is small, so, still many of these levels contributed to the Raman scattering. We consider such a scattering as non-resonant (see section 3.1).

The Raman spectra are exposed in figure 2 according to different crystalline quality of the semiconductor phase in the samples, which decreases from the top to the bottom. The spectrum of the film where, according to the XRD data, it is least crystalline (A4-2, shown in the inset) displays just a broad band, centred at about 300 cm^{-1}. The intensity of this band is quite low compared to the peaks seen for the other samples. Such a band is typical of amorphous systems [19] where the Raman cross-section is proportional to the total density of vibrational states rather than to the spectral density of long-wavelength phonons [20]. The lineshape of the optical phonon peak originating from semiconductor nano-crystallites (NCs) is rather asymmetric for all the films studied, which is characteristic of NC systems (e.g. [1, 5, 12]). As we will see in the next section, this can be understood within any model which properly considers the confinement of optical vibrons in sufficiently small nano-crystallites. However, such a large broadening of the Raman peak as seen for the A4-33 and A4-6 samples (figure 2) cannot be explained without involving intrinsic disorder in the NCs.

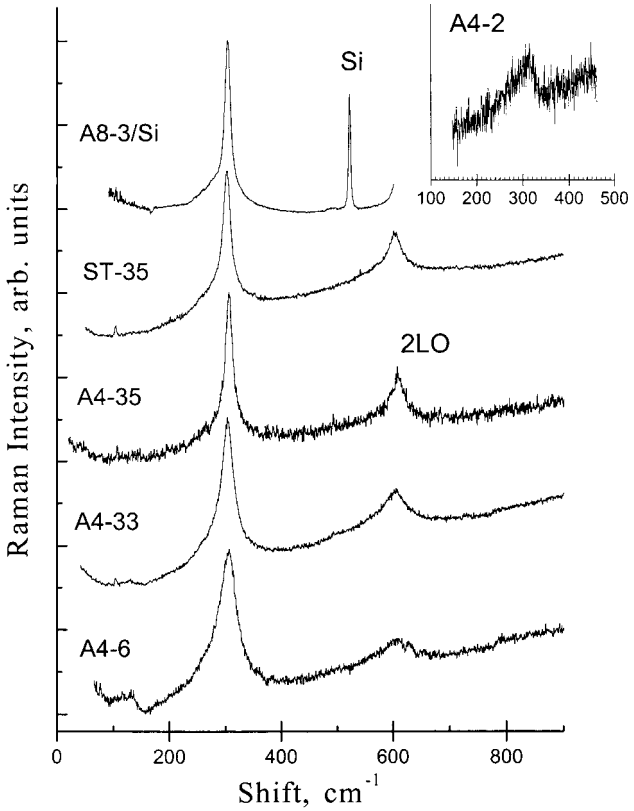

Figure 2. Experimental Raman spectra of several CdS-doped films ($\lambda_{ex} = 514$ nm). The spectra are displayed according to a decrease of the crystalline quality from the top to the bottom (see also table 1). The inset shows a broad amorphous-like band in the Raman spectrum of a film annealed at the lowest temperature (300 °C). The peak in the spectrum of the A8-3/Si designated as 'Si' originates from the silicon substrate (all other samples presented here were grown on SiO_2 substrates). The feature marked '2LO' is due to scattering on two LO-type confined phonons.

3. Theoretical background and spectrum modelling

3.1. Spherical model

Optical phonons in a sphere were considered in detail in [9] on the basis of a continuum equation of motion for the relative displacement of two sublattices of a zinc-blende structure semiconductor. Raman scattering on these modes was studied theoretically in [10, 11] for the Fröhlich interaction of confined electrons and phonons with vibrons, and in [12] within a phenomenological model. Here we generalize this model also for the case of the deformation potential interaction.

The Raman cross-section can be written in the following form:

$$\frac{\mathrm{d}^2\sigma}{\mathrm{d}\Omega\,\mathrm{d}\omega_S} = \frac{\omega_I\omega_S^3 v^2}{\pi c^4}[n(\omega)+1]\left\{-\mathrm{Im}\sum_{\nu}\frac{|\Theta_\nu|^2}{\omega-\omega_\nu+\mathrm{i}\Gamma_{LO}}\right\} \tag{1}$$

where v is the unit cell volume, I and S correspond to the incident and scattered light, respectively, $n(\omega)$ is the Bose factor, $\omega = \omega_I - \omega_S$, Γ_{LO} is a damping parameter, ν enumerates phonon eigenstates and Θ_ν is a scattering matrix element which will be considered below.

Off resonance with any particular electron–hole (e–h) pair state, it is sufficient to consider just spherical phonon modes [22], i.e., $\nu \Rightarrow l = 0, n = 1, 2, \ldots$. Their frequencies are given by

$$\omega_n^2 = \omega_{LO}^2 - \beta_{LO}^2 \left(\frac{\zeta_n}{R_0}\right)^2 \tag{2}$$

where ω_{LO} and β_{LO} are the bulk LO phonon frequency and LO phonon dispersion curve bending parameter, respectively, R_0 is the sphere's radius and ζ_n is the nth root of the first spherical Bessel function j_1. The latter is the $l = 0$ solution of the equation of motion [9] with rigid mechanical boundary conditions (b.c.s):

$$w_n(\vec{R}) = \frac{(2v)^{1/2}}{(4\pi)^{1/2} R_0^{3/2}} \frac{j_1(\zeta_n R/R_0)}{|j_0(\zeta_n)|} \tag{3}$$

where the coefficient is a normalization constant. A factor of $(\hbar/(2\mu\omega))^{1/2}$ must be added if one considers a vibration quantum (μ is the reduced mass).

The matrix element in (1) describes the non-polar (via the deformation potential) or polar (via the Fröhlich electric field) scattering of electrons and holes on the vibrons. For the latter case, within the effective mass approximation, it can be written as follows (e.g. [20]):

$$\Theta_n = -\frac{e^2}{m_0^2 \omega_I \omega_S} \sum_{i,f} \frac{(\vec{P}_{0i}\vec{e}_I)(\vec{P}_{f0}\vec{e}_S)}{(E_i - \hbar\omega_I)(E_f - \hbar\omega_S)} \times \int (-e\phi_n(\vec{R}))[\Psi^{e*}{}_f(\vec{R})\Psi^e{}_i(\vec{R}) - \Psi^{h*}{}_f(\vec{R})\Psi^h{}_i(\vec{R})]\,\mathrm{d}\vec{R} \tag{4}$$

where i and f refer to e–h pair states before and after scattering on a phonon, $\vec{P}$ is the momentum matrix element, $\vec{e}_{I,S}$ are the polarisation vectors, Ψ is the electron or hole envelope wavefunction and ϕ_n is the potential associated with the nth phonon mode,

$$e\phi_n = \frac{2^{1/2}}{|j_0(\zeta_n)|} \frac{C_F}{\zeta_n} [j_0(\zeta_n) - j_0(\zeta_n R/R_0)] \tag{5}$$

$$C_F = e\sqrt{2\pi\hbar\omega_{LO}(\epsilon_\infty^{-1} - \epsilon_0^{-1})R_0^{-1}}$$

ϵ_∞ and ϵ_0 are the high-frequency and static dielectric constants of the semiconductor, respectively and j_0 is the 0th spherical Bessel function. Note that the normalization factor is missing in the expression for the potential given in [9, 11].

The optical deformation potential acting on electrons in zinc-blende semiconductors is proportional to the change in the bond length [21]. Its matrix element is:

$$H_{fi} = \frac{1}{2}\frac{d_0}{a_0} \int (\vec{e}_l \vec{w}(\vec{R}))\Psi^*{}_f(\vec{r})\Psi_i(\vec{r})\mathrm{d}\vec{R} \tag{6}$$

where d_0 is a deformation potential constant (which, in the Γ-point, is non-zero only for the valence band), a_0 is the lattice constant and $\vec{e}_l$ is a unit vector along the (111) direction. Within the continuum model, we shall consider the radial component of $\vec{w}$ (3) as the change of the bond length. The result of substituting (3) into (6) replaces the second line in (4) for this case.

If the excitation energy $\hbar\omega_I$ falls well above the absorption edge and corresponds to the quasiclassical region of the QD e–h spectrum, we can approximate

$$\Psi^{e,h*}{}_f(\vec{R})\Psi^{e,h}{}_i(\vec{R}) \approx \frac{\text{const}}{R_0^3}\delta_{if} \tag{7}$$

and neglect the difference in the denominator in (5) for different e–h states. Then we obtain from (4), (5) and (3), (6):

$$|\Theta_n|^2 \sim N^2 \begin{cases} C_1 (C_F)^2 \zeta_n^{-2} & \text{(polar)} \\ C_2 \dfrac{\hbar}{\rho \omega_{LO}} \left(\dfrac{d_0}{a_0}\right)^2 R_0^{-3} \left[\dfrac{2(1-\cos\zeta_n) - \zeta_n \sin\zeta_n}{\zeta_n^2 \sin\zeta_n}\right]^2 & \text{(non-polar)} \end{cases} \tag{8}$$

where C_1 and C_2 are constants, $\rho = \mu/v$ and N is the number of e–h pair states contributing to the Raman scattering.

In the quasiclassical approximation, $N \sim R_0^3$ and

$$|\Theta_n|^2(R_0) \sim R_0^5 \qquad \text{and} \qquad |\Theta_n|^2(R_0) \sim R_0^3$$

for the Fröhlich and deformation potential scattering, respectively. The latter corresponds to the macroscopic model result [12], where the cross-section is proportional to the crystal volume. The relative weights of different confined modes (the second line in (8)) are also the same as in [12]. This corresponds, for example, to the experimental situation of [8].

If the excitation energy is below the absorption edge, several e–h states can give comparable contributions to the scattering. We can estimate the scattering matrix element using the model of [23]. In this model, the mixing of different hole subbands is neglected and (for an infinitely high potential barrier between semiconductor and glass) the electron and hole envelope wavefunctions are

$$\begin{aligned} \Psi^{e,h}_{NLM} &= R_0^{-3/2} \mathrm{R}_{NL}(R) Y_{LM}(\Omega) \\ \mathrm{R}_{NL}(R) &= \sqrt{2} \frac{j_L(\zeta_{NL} R/R_0)}{|j_{L+1}(\zeta_{NL})|} \end{aligned} \tag{9}$$

where ζ_{NL} is the Nth root of the Lth spherical Bessel function and $Y_{LM}(\Omega)$ is the (normalized) spherical harmonic. Accordingly, the e–h energy levels are given by

$$E_{NL}(R_0) = E_g + \frac{\hbar^2 (\zeta_{NL})^2}{2R_0^2} \left(\frac{1}{m_e} + \frac{1}{m_h}\right) \tag{10}$$

where E_g is the band gap energy and m_e and m_h are the electron and hole effective masses, respectively. Then the Raman scattering matrix element can be calculated according to

$$|\Theta_n|^2(R_0) = \frac{1}{16\pi R_0^3} \left(\frac{e^2 P^2 d_0}{m_0^2 \omega_I \omega_S a_0}\right)^2 \left| \sum_L \sum_{N,N'} \frac{B^n_{N,N';L}}{(E_{NL}(R_0) - \hbar\omega_I)(E_{N'L}(R_0) - \hbar\omega_S)} \right|^2 \tag{11}$$

with

$$B^n_{N,N';L} = R_0^{3/2} (2L+1) \int_0^1 R_{NL}(x) R_{N'L}(x) w_n(x) x^2 \, \mathrm{d}x.$$

The relative contributions of different confined modes calculated using (9)–(11) are shown in figure 3 for $\hbar\omega_I = 2.4$ eV. They are different from those given by the second line of (8) (and shown in the inset in figure 4) but are similar in the sense that the $n > 1$ mode's contributions are at least one order of magnitude less than that of the $n = 1$ mode. It scales with sphere's size approximately as R_0^4 for the indicated value of the excitation energy.

For the Fröhlich mechanism, such an estimate is not possible, because the matrix element is exactly equal to zero within the model of [23]. It is non-zero if one takes into account the hole subband mixing. This results in the appearance of a number of closely spaced hole levels with different angular and radial dependence of the envelope wavefunctions [24]. So, (7) may be not a bad approximation for this situation.

Experimentalists almost always deal with ensembles of nano-crystallites rather than with a single QD. Since confined optical vibrons produce neither mechanical nor electric field outside

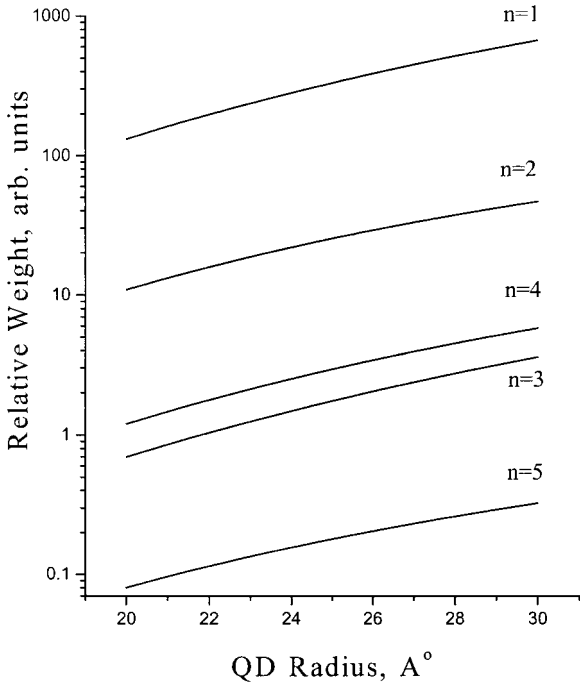

Figure 3. Squared scattering matrix element against QD radius calculated according to (9)–(11) for the first five confined vibron modes. The excitation energy $\hbar\omega_I = 2.4$ eV corresponds to the green line of an Ar^+ laser.

the QD, the total Raman cross-section of an ensemble of spheres is simply an average of the individual QD contributions:

$$\frac{\mathrm{d}^2\sigma}{\mathrm{d}\Omega\,\mathrm{d}\omega_S} \sim [n(\omega)+1]\int dR_0 F(R_0)\left\{-\mathrm{Im}\sum_n \frac{|\Theta_n|^2(R_0)}{\omega-\omega_n(R_0)+\mathrm{i}\Gamma_{LO}}\right\} \qquad (12)$$

where $F(R_0)$ is the distribution function of sphere size, which depends on the preparation method [25].

The results calculated using this model are given in figures 4–7. The necessary bulk phonon parameters were taken from the literature [10] and the values of the phonon damping, mean value and standard deviation of the Gaussian distribution of sphere radius assumed which were used in the calculations are given in table 1. In the experimental spectra, a frequency-dependent background of the form $A + B\omega$ owing to fluorescence was substracted.

For the A4-35 sample ($\bar{R}_0 \approx 30$ Å, figure 4), one of the best in terms of the crystalline quality, the peak and its asymmetry are rather well reproduced by the model, the agreement being slightly better assuming the Fröhlich mechanism. It is difficult to estimate the relative importance of the two mechanisms because the constants C_1 and C_2 in (8) are unknown and different. (Note that the scattering matrix element is proportional to the difference between the electron and hole contributions for the Fröhlich mechanism, while there is no electron scattering for the optical deformation potential one.) Although the relative weights of the modes with $n > 1$ differ considerably for the two mechanisms (see the inset in figure 4), the resulting spectra are not so distinct because of the relatively small β_{LO} in CdS.

The agreement is poorer for the St-35 (figure 5) and A8-3/Si (figure 6) samples, although they do not look much different from the A4-35 in terms of XRD, except for the smaller QD

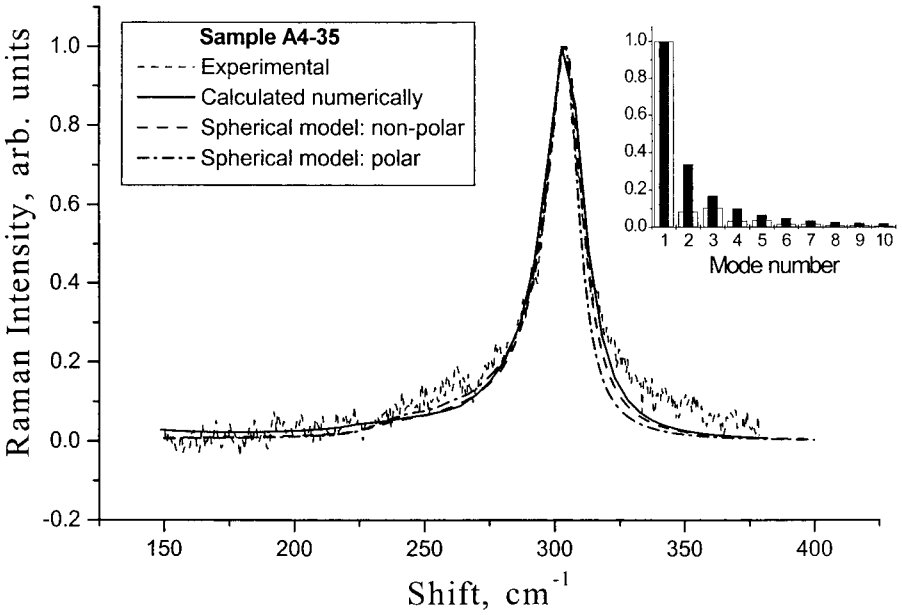

Figure 4. Raman lineshape for an RF-sputtering-grown sample A4-35: experimental (fine broken curve) and calculated using the spherical model (bold broken curve) and numerically (full curve). The relative contributions of different confined spherical modes calculated according to (8) are shown in the inset (with empty and black bars for the deformation potential and Fröhlich mechanisms, respectively). $\Gamma_{LO} = 7$ cm^{-1} and a Gaussian distribution of sphere radii with $\bar{R} = 30$ Å and $\sigma R = 6$ Å were used in the fitting. In the numerical calculation, $\Gamma_{LO} = 6$ cm^{-1}, round clusters with $D = 18$ monolayers (ML) and a Gaussian distribution of the n-n force constants with a relative standard deviation of 0.05 were assumed.

size ($\bar{R}_0 \approx 20$ Å for both). Although the peak is well reproduced using reasonable values of Γ_{LO} and σR (see table 1), the experimental lineshape has a 'pedestal' not described by the model. A similar discrepancy for the low-frequency wing seems to be present also in most of the published Raman spectra [1, 5, 7, 8]. Usually this was explained by an eventual contribution of the $l = 2$ spheroidal vibron modes or even dipolar $l = 1$ modes activated by the presence of impurities or defects [1, 7, 10]. However, this can happen only under resonance conditions, which were not the case in our experiments. It is even harder to explain the high-frequency shoulder seen in figure 5 *above* the bulk LO frequency. There are, in fact, only two possibilities, (i) incorporation of a light impurity (most likely Zn) into the nano-crystallites [25] and (ii) compressive strain [26]. They will be considered in the next section.

The broader spectrum of the A4-33 sample can reasonably well be fitted with this model (see figure 7). However, it requires an unrealistically large value of the homogeneous broadening $\Gamma_{LO} = 11$ cm^{-1} and a very broad QD size distribution. We believe that this large broadening is not homogeneous and reflects a significant disorder in individual nano-crystallites. The same applies to the A4-6 sample whose Raman spectrum, strictly speaking, cannot be described at all by the model considered in this section because the peak frequency is higher than the bulk ω_{LO}.

3.2. Clusters of arbitrary shape

To study the vibrational properties of clusters of arbitrary shape or with some atomic disorder, one needs to solve numerically the appropriate microscopic equations of motion. This means a

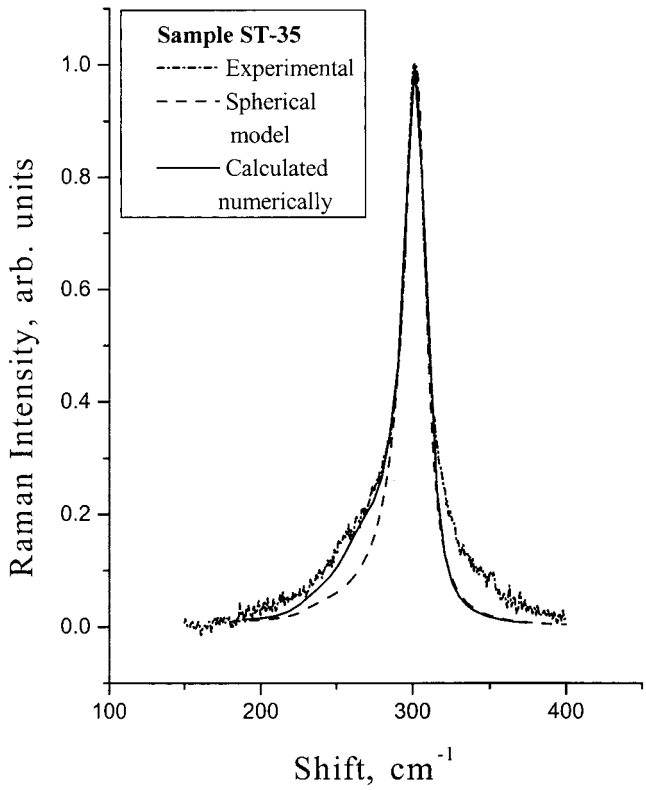

Figure 5. Raman spectra for a 'sol–gel'-grown sample St-35: experimental (broken curve, the whole spectrum is shown in figure 2) and calculated using the spherical model (dashed curve) and numerically (full curve). See tables 1 and 2 for the parameters used in the spherical model and numerical calculations, respectively.

diagonalization of the corresponding dynamical matrix. The main difficulty is that, in general, it is necessary to know all eigenvalues and eigenvectors of the dynamical matrix to calculate the observable properties (like the Raman cross-section) for a system with disorder. To be able to consider clusters of sufficient size, we studied the problem in two dimensions. We hope that the results obtained from such a modelling are useful since the dimensionality is not so critical in this case as it is, for example, in the problem concerning the conductivity of disordered systems.

We took into account the short-range interatomic interaction in the spirit of the Keating model [27]. The nearest-neighbour interaction constant could be considered as a random variable with a certain (e.g. Gaussian) distribution in order to model random atomic deviations from the regular lattice positions. The Coulomb interaction must be treated in a special way in 2D, in order to reproduce the LO–TO splitting at the Brillouin zone centre. The Coulomb force constants were taken according to

$$\begin{aligned} \overleftrightarrow{F}_{ij} &= \pm A^2(1-\delta_{ij})\frac{2\vec{e}_{ij}\vec{e}_{ij} - \overleftrightarrow{1}}{R_{ij}^2} \\ \overleftrightarrow{F}_{ii} &= -\sum_j \overleftrightarrow{F}_{ij} \end{aligned} \tag{13}$$

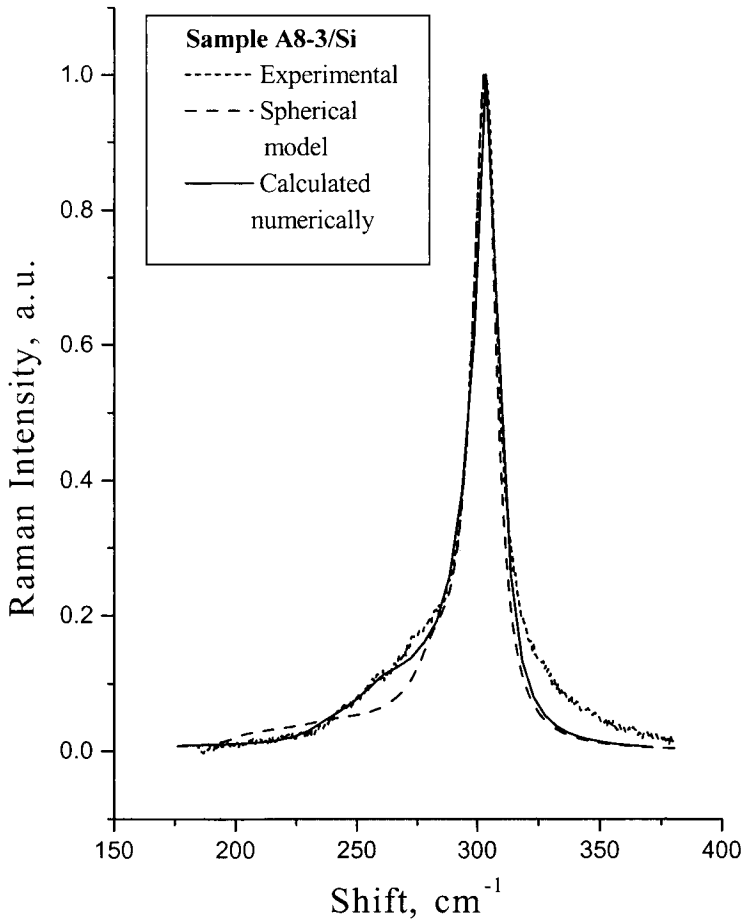

Figure 6. Raman spectra for the A8-3/Si sample (same key as for figure 5).

where $\vec{R}_{ij} = R_{ij}\vec{e}_{ij}$ is the radius-vector between two lattice sites i and j, $\overleftrightarrow{1}$ is a 2D diadic

$$A^2 = \frac{\mu s}{2\pi}(\omega_{LO}^2 - \omega_{TO}^2)$$

and s is the unit cell area. In (13), $(\pm)$ applies to pairs of like or unlike atoms, respectively. Such a dipole–dipole interaction tensor (13) corresponds to a 2D 'Coulomb' potential $\pm A^2 \ln R$. It can be shown that such an interaction leads to a symmetric LO–TO splitting at the Brillouin zone (BZ) centre of an infinite 2D crystal with respect to

$$\omega_0^2 = \tfrac{1}{2}(\omega_{LO}^2 + \omega_{TO}^2).$$

The ω_0^2 is determined by the short-range interaction. We chose these interaction constants to get $\omega_0 \approx 275$ cm^{-1} for CdS. In order to simplify the treatment of the electromagnetic interaction across the cluster/matrix interface, we assumed that the clusters are embedded in a host with same (background) high frequency dielectric constant and the host material is not polarisable at frequencies characteristic of CdS vibrational modes.

Clusters of arbitrary shape were generated on a square lattice from a perfect binary supercell replacing some Cd and S atoms by very heavy chargeless particles. This way we were able to consider 'regular' (round) crystallites as well as irregular shape clusters having

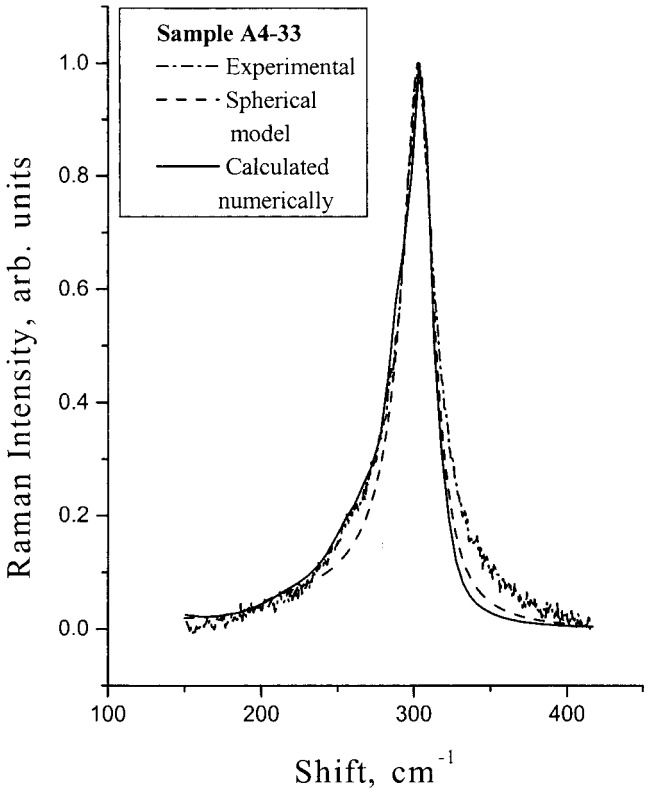

Figure 7. Raman spectra for the A4-33 sample (same key as for figure 5).

random mounds on the surface. Two kinds of mechanical boundary condition (b.c.) were considered: (i) rigid and (ii) free (with some dangling bonds for atoms at the cluster edges). Results obtained using these different b.c.s are compared in figure 8. Otherwise, all the spectra presented were calculated using rigid b.c.s (i).

Once the dynamical matrix of such a cluster was constructed and its eigenvalues ω_ν^2 and eigenvectors $\vec{u}_\nu$ were obtained using the QR algorithm, the Raman cross-section was calculated according to (1) with

$$\Theta_\nu = C\sum_i (-1)^i \left\{ \sum_j (-1)^j (1-\delta_{ij}) \frac{[M_i^{-1/2}\vec{u}_\nu(i) - M_j^{-1/2}\vec{u}_\nu(j)]\vec{e}_{ij}}{R_{ij}^2} \right\} \quad (14)$$

where C is a constant and M_i are atomic masses. The sum over j represents the potential created by all the vibrating atoms at a lattice site i.

Figure 6 shows the calculated Raman spectra of several 'round' clusters of different size without disorder. The peak shifts downwards and broadens (if normalized in intensity) when the cluster size decreases, just as in the 'spherical' model. Applying free b.c.s (which can be relevant for QDs suspended in a liquid) produced a surface mode below $\omega_{TO} = 240$ cm^{-1} due to the dangling bonds, while the peak does not change much (dashed curve in figure 8). This mode should not be confused with those predicted by the continuous model [9] (spherical modes with $l \geqslant 1$ are also sometimes called surface modes). These latter vibrations always have frequencies within the phonon band of the bulk material.

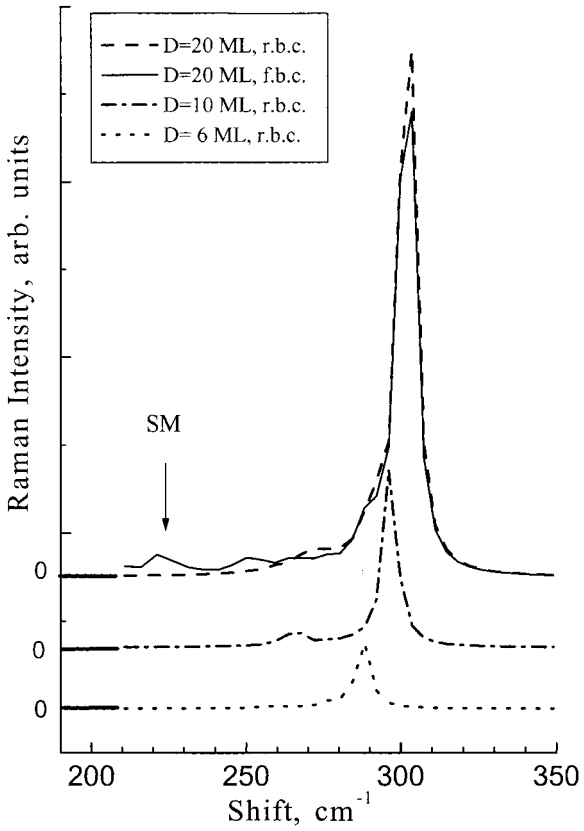

Figure 8. Calculated Raman intensity for round clusters of different diameter. The full curve was calculated for $D = 20$ ML using free b.c.s, while rigid b.c.s were used for all the others. SM marks the surface mode produced by superficial atoms with dangling bonds.

Let us turn to disorder in a single nano-crystallite, in which we considered two kinds. First, we assumed that the cluster's shape can be quite irregular although the material is crystalline. Clusters of irregular shape were constructed by disordering some m ($m = 1, 2, \ldots$) superficial layers with the probability decreasing linearly from the surface to the centre of the cluster. An example of such a cluster can be seen in the inset in figure 9, where also some calculated spectra are shown. For clusters with disorder, the Raman intensity was averaged over several different shape realizations. As can be seen from figure 9, 'shape disorder' leads to an asymmetric broadening of the Raman peak. (Of course, the intensity also decreases, but it is difficult to compare its absolute values in experiment. This is why we normalized the spectra to the peak value.) Another effect seen for clusters with strongly disordered shape is the appearance of a low-frequency mode originating from BZ edge acoustic vibrations. Such modes (called DALA or DATA—disorder-activated acoustic modes) are frequently observed in Raman spectra of pseudobinary alloy materials [28] including QDs [14]. It seems that this mode was also observed recently for CdS_xSe_{1-x} nano-crystallites [8], where it is activated by composition disorder.

Another factor beyond the model of section 3.1 is concerned with possibly imperfect atomic order in nano-crystallites. We considered a 'hot solid state' model, which is an atomic system with the topology of a regular crystal lattice but with random interatomic distances (or,

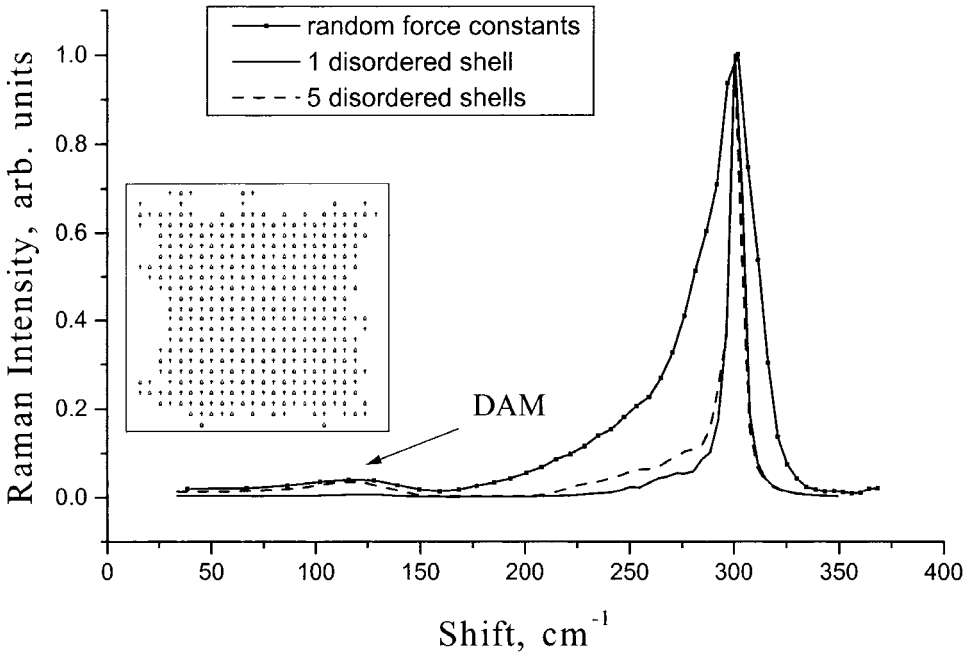

Figure 9. Numerically calculated Raman intensity for a cluster with $D = 30$ ML and one or five disordered shells. A typical cluster used in these calculations is shown in the inset. The curve with points corresponds to an ensemble of round ($D = 20$ ML) clusters with a Gaussian distribution of the n-n force constants. It was obtained by averaging over some 30 realizations. DAM stands for disorder-activated acoustic mode.

equivalently, with random short-range force constants) [29]. Such disorder in NCs can appear as a result of quenching. Moreover, compressive strain caused by the matrix and detected in several studies of semiconductor-doped glasses [26] can lead also to a systematic shift of the CdS bond frequency.

An example of such a calculation with Gaussian-distributed nearest-neighbour (n-n) force constants is also shown in figure 9. The spectra of individual clusters with the 'hot solid state' kind of disorder have a lot of features, which are smoothed out when averaged over a few tens of realizations. A sufficiently large ensemble of different realizations should contain some nearly amorphous clusters. As expected, this kind of disorder (even with a distribution of the force constant unshifted with respect to the 'crystal' value) produces some Raman-active vibrational modes above ω_{LO}.

Despite the fact that the model considered in this section is too coarse to describe the full lattice dynamics of a real 3D crystal, we tried to fit some of our experimental spectra using the numerically calculated quantities. Assuming a certain degree of the interface roughness and a Gaussian distribution of the n-n force constants with different standard deviation (see table 2), we were able to fit most of our Raman spectra. The degree of accuracy in the reproduction of the Raman lineshape is similar to that provided by the 'spherical' model for most crystalline samples (see figure 4). The force constant variation assumed for this sample is quite small and the effect which it produces on the lineshape cannot be distinguished from that of the QD size distribution within the spherical model. On the contrary, in the case of the A4-33 sample (figure 7) the disorder effects seem to be a plausible explanation for the observed lineshape (compare parameters from tables 1 and 2 used for the fitting).

Table 2. Parameters used in the numerical lattice dynamics calculations.

Sample	Γ_{LO} (cm^{-1})	Cluster core size (ML)	Number of disordered shells/ excluded atoms	N-n force constant dispersion
A4-6	9	24	3/60	$\sigma f/\bar{f} = 0.3$
A4-33	8	14	—	$\sigma f/\bar{f} = 0.25$
A4-35	7	18	—	$\sigma f/\bar{f} = 0.05$
A8-3/Si	7	14	2/25	—
St-35	8	14	3/60	—

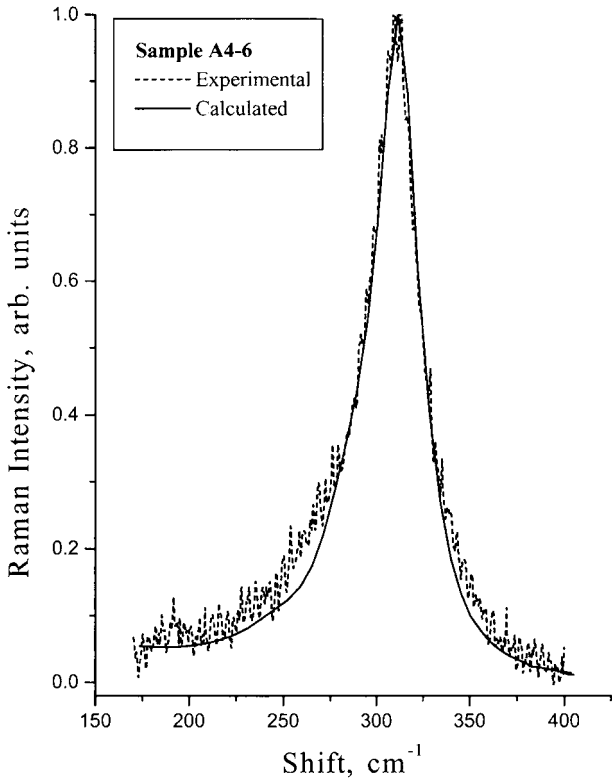

Figure 10. Raman spectra for the A4-6 sample: experimental (broken curve) and calculated numerically (full curve). A shifted Gaussian distribution of n-n force constants corresponding to a mean Cd–S bond vibrational frequency of $\bar{\omega}_0 = 284\ cm^{-1}$ was assumed.

For the St-35 (figure 5) and A8-3/Si samples (figure 6), there was no significant n-n force dispersion assumed, because the central part of the peak is rather narrow. The low-frequency wing was modelled assuming just shape disorder for both of them.

A good fit to the spectrum of the A4-6 sample was achieved assuming a quite broad and shifted Gaussian distribution of the n-n force constants together with some interface roughness (figure 10). As for the A4-2 sample, its semiconductor phase is probably not crystalline at all and cannot be described by the 'hot solid state' model.

4. Discussion and conclusions

We studied experimentally a set of CdS-doped glass films prepared at different temperatures. Accordingly, the crystalline quality of the semiconductor phase varied for different samples. HRTEM studies made on some of them revealed the presence of nearly spherical nano-crystallites. So, we expected that the 'spherical' model of phonon confinement considered in section 3.1 would adequately describe the experimental Raman spectra of such samples. We developed this model proposed in [9–11] by including the deformation potential scattering. In fact, it reproduced reasonably well the shape of the peak for the most crystalline A4-35, St-35 and A8-3/Si samples (figures 4–6). However, even in these cases there are further effects contributing to the scattering.

One can argue that, as the size distribution function is not exactly known, an appropriate choice of this function could provide a better fit to the spectra. In fact, this is not so. We tried Gaussian, Lifshitz–Slyozov and some other distribution functions.The shape of the spectrum does not change much unless one invents an exotic function. QDs of sizes smaller than the mean one contribute little to the scattering under non-resonant conditions (see formula (8) and its discussion).

As we have mentioned in section 3.1, the deviation in the low-frequency part of the band (between 240 and 270 cm^{-1}) is usual for QD systems. The most common explanation to this involves the $l = 2$ spheroidal vibron modes, which indeed should contribute to the scattering under resonant conditions. However, our calculations [30] show that only those of them whose frequencies lie between that of the so called quadrupole electrostatic surface mode ($\approx$285 cm^{-1} for CdS in SiO_2) and ω_{LO} should contribute efficiently to the scattering.

Another explanation was proposed in [12], where the extra scattering was associated with a collective polariton mode involving many QDs and occuring approximately at the Fröhlich frequency ($\approx$278 cm^{-1}). However, in a recent work [31] we found a similar discrepancy for Ge-doped glasses, where there is no such polariton. It was argued that the difference between the experimental spectrum and the theoretical one calculated assuming only scattering on Ge nano-crystallites was due to an amorphous semiconductor phase present in the Ge-doped glass films studied in [31].

Such a mode, additional to one produced by low-wavenumber LO-type phonons, was also discussed in [8] with respect to glasses doped with Cd(SSe) nano-crystallites. The authors of this work assigned this mode to be a BZ edge LO phonon activated by composition disorder, as observed also in Raman spectra of CdS_xSe_{1-x} single crystals. Indeed, the similarity of the spectra of bulk and nano-crystalline samples reported in [8] is remarkable, demonstrating that the effect of disorder can surpass that of the quantum confinement.

Direct correlation between the broadening of the Raman lineshape and the crystalline quality of the CdS phase dispersed in glass revealed by the present study leads us to the conclusion that disorder has the most important effect on the Raman scattering in this material. There are mainly four sources of disorder in semiconductor-doped glasses. First, the semiconductor phase may be unintentionally doped. Our XPS studies of the chemical composition of the films did not reveal the presence of impurities in concentrations which could affect significantly the lattice dynamics of the nano-crystallites. However, only a thin superficial layer is probed by this technique and some QD could still be contaminated by impurities from the substrate (the most probable candidate is Zn [25]). Secondly, different nano-crystallites can have slightly different properties because of fluctuations in the matrix. For example, they can be subject to fluctuating stresses. Thirdly, the particle's shape can be randomly irregular, particularly in samples grown and processed at relatively low temperatures. Such shape irregularities can be seen in the TEM image of figure 1. Lastly, the interatomic

distances and bond angles can fluctuate inside one nano-crystallite. If the fluctuations are small, one still can think in terms of a crystal lattice (the 'hot solid state' model). If this is not so, the semiconductor phase is amorphous. (In fact, it is the distribution of bond angles that broadens considerably in amorphous materials compared to crystals, while the n-n interatomic distance does not change much [32]. Our lattice dynamics model described in section 3.2 is too simple to describe a real amorphous material. This is why we confine ourselves by the 'hot solid state' model although believing that the calculated results can be extrapolated to amorphous particles.) Probably XRD spectroscopy cannot distinguish between this and the shape disorder, because both lead basically to some broadening of the crystal structure peaks. The XRD lineshape should be, of course, different in the two cases, but, in practical terms, it is difficult to tell one from the other. TEM would also have difficulties revealing particles with interatomic distance disorder. However, Raman spectroscopy should be able, in principle, to distinguish shape and interatomic distance disorder, following from our calculated results presented in section 3.2.

What we tried to show by means of our model lattice dynamics calculations on random clusters is that these different kinds of disorder can lead to somewhat different consequences in terms of vibron modes and, consequently, Raman spectra. Doping CdS nano-crystallites with Zn in random concentrations would result in random upward shifts of the vibron frequencies. (CdZn)S is a one-mode alloy where the phonon frequencies depend almost linearly on the composition [33]. The one-mode behaviour cannot be modelled adequately in two dimensions [34], because any lattice defect necessarily produces a local vibrational mode in 2D. Phenomenologically, the result of the random doping of CdS nano-crystallites with Zn should be similar to that of subjecting them to random compressive strains. By allowing the Cd–S bond frequency ω_0 to be a random variable for different QDs in the ensemble, we expected to model these two kinds of disorder. Indeed, some density of Raman-active vibrational states appeared above the CdS LO phonon frequency, but we were not able to reproduce the experimental lineshape in this region of the spectrum (for example, for the A4-33 sample, figure 7). Studies of the chemical composition and strain across the film would be necessary to tackle properly these effects.

The other two kinds of disorder are inherent for individual nano-crystallites. In the 'irregular shape' model, the cluster fringes play the role of small QDs and produce a low-frequency tail of the Raman peak. This effect is similar to one discussed in [13], where random fluctuations of the QD shape contribute to the spread of electronic levels seen in the experiments. Moreover, some acoustic vibrations corresponding to the BZ edge of the bulk crystal become Raman-active when localized in very small 'peninsulas' of the nano-crystallites. A similar effect is seen in Raman spectroscopy of semiconductor alloys [28, 33] and was reported recently for nano-crystalline CdS_xSe_{1-x} [8]. One can see a weak feature at approximately 130 cm^{-1} in the spectrum of the A4-6 sample (figure 2), which can be associated with the DALA mode. Using the resonant Raman effect should help with the identification of this mode in QD systems.

A random distribution of the n-n force constants leads to an asymmetric broadening of the Raman peak and also produces the disorder-activated acoustic mode (figure 9). Surprisingly, the intensity drops very abruptly to the higher shift side, although some states do appear above the bulk LO phonon frequency. The peak is much broader than for perfectly crystalline QDs but its shape is similar. We think that this model, which incorporates the confinement effect and fluctuations of interatomic distances, describes the main sources of the broadening of the Raman lineshape in small clusters produced by a low-temperature technique. It also explains the spectra where the peak is shifted upwards with respect to ω_{LO} (figure 10). Further HRTEM experiments, which are under progress now, may help to confirm the presence of this kind of

disorder in II–VI nano-crystallites. Perhaps with a most realistic distribution function of the force constants one can obtain a better fit of the high-frequency shoulder appearing in the spectra of samples similar to A4-33 (figure 7).

It should be borne in mind, of course, that one can not completely trust the disorder parameters (listed in table 2) obtained by the line shape fitting using a 2D lattice dynamics model. Obviously, more elaborate 3D calculations are needed to extract quantitative information concerning disorder from the Raman spectra. However, we believe that, qualitatively, the results of our numerical simulation are relevant to reality.

In conclusion, we considered the effects of disorder in nano-crystallites on their Raman spectra. We have demonstrated, by means of our model calculations, how different kinds of disorder in QD systems should manifest themselves in the spectra. From the point of view of characterization of semiconductor doped glass films, Raman spectroscopy was shown to allow for rapid conclusions concerning the crystalline quality of the semiconductor phase from the broadening of the optical phonon peak. If fitting the spectral lineshape using the spherical model requires too high values of the phonon damping, it means that the broadening is *inhomogeneous*. This broadening is most likely caused by fluctuations of the n-n force constant within one nano-crystallite. Shape disorder (interface roughness) does not change significantly the central part of the peak but produces a noticable low-frequency tail within the optical phonon band of the bulk material. By modelling the lineshape, it is possible to obtain semi-quantitative conclusions concerning the type and degree of disorder present in the nano-crystallites. Under resonance conditions, one should also be able to detect another sign of disorder, namely, the low-frequency mode originating from BZ edge acoustic vibrations and activated either by shape irregularities or imperfect crystalline order in nano-particles.

Acknowledgments

This work was supported by FCT, Portugal (project PRAXIS/C/FIS/10128/1998). The authors are grateful to Dr G Hungerford for a critical reading of a manuscript.

References

[1] Trallero-Giner C, Debernardi A, Cardona M, Menendez-Proupin E and Ekimov A I 1998 *Phys. Rev.* B **57** 4664
[2] Woggon U 1996 *Optical Properties of Semiconductor Quantum Dots (Springer Tracts in Modern Physics vol 136)* (Berlin: Springer) ch 10
[3] Klein M C, Hache L, Ricard D and Flytzanis C 1990 *Phys. Rev.* B **42** 11 123
[4] Tognini P, Andreani L C, Geddo M, Stella A, Cheyssac P, Kofman R and Migliori A 1996 *Phys. Rev.* B **53** 6992
[5] Roy A and Sood A K 1996 *Phys. Rev.* B **53** 12 127
[6] Nanda K K, Sarangi S N, Sahu S N, Deb S K and Behera S N 1999 *Physica* B **262** 31
[7] Hwang Y N, Park S H and Kim D 1999 *Phys. Rev.* B **59** 7285
[8] Ingale A and Rustagi K C 1998 *Phys. Rev.* B **58** 7197
[9] Roca E, Trallero-Giner C and Cardona M 1994 *Phys. Rev.* B **49** 13 704
[10] Chamberlain M P, Trallero-Giner C and Cardona M 1995 *Phys. Rev.* B **51** 1680
[11] Menendez E, Trallero-Giner C and Cardona M 1997 *Phys. Status Solidi* b **199** 81
[12] Vasilevskiy M I, Rolo A G and Gomes M J M 1997 *Solid State Commun.* **104** 381
[13] Tsiper E V 1996 *Phys. Rev.* B **54** 1959
[14] Sirenko A A, Zundel M K, Ruf T, Eberl K and Cardona M 1998 *Phys. Rev.* B **58** 12 633
[15] Rolo A G, Vieira L G, Gomes M J M, Ribeiro J L, Belsley M S and Dos Santos M P 1998 *Thin Solid Films* **312** 348
[16] Rolo A G, Conde O and Gomes M J M 1998 *Thin Solid Films* **318** 108
[17] Othmani A, Plenet J C, Bersstein E, Bovier C, Dumas J, Riblet P, Gillot P, Levy R and Grun J B 1994 *J. Cryst. Growth* **144** 141

[18] Rakovitch Yu P, Rolo A G, Stepikhova M A, Vasilevskiy M I, Gomes M J M, Artemyev M V, Jantsch W, Heiss W and Prechtl G 2000 *Mater. Res. Soc. Symp. Proc.* vol 571 (Warrendale, PA: Materials Research Society) p 69
[19] Alben R, Weaire D, Smith J E and Brodsky M H 1975 *Phys. Rev.* B **11** 2271
[20] Hayes W and Loudon R 1978 *Scattering of Light by Crystals* (New York: Wiley) ch 3
[21] Blacha A, Presting H and Cardona M 1984 *Phys. Status Solidi* b **126** 11
[22] Duval E 1992 *Phys. Rev.* B **46** 5795
[23] Efros Al L and Efros A L 1982 *Sov. Phys.–Semicond.* **16** 772
[24] Grigoryan G B, Kazaryan E M, Efros Al L and Yazeva T V 1990 *Sov. Phys.–Solid State* **32** 1031
[25] Yukselici H, Persans P D and Bilodeau T G 1995 *Phys. Rev.* B **52** 11 763
[26] Zhao X S, Schroeder J, Persans P and Bilodeau D 1991 *Phys. Rev.* B **43** 12 580
[27] Keating P N 1966 *Phys. Rev.* **145** 637
[28] Talwar D N and Fang T D 1989 *Phys. Rev.* B **41** 3746
[29] Ziman J M 1979 *Models of Disorder* (Cambridge: Cambridge University Press) ch 2
[30] Vasilevskiy M I *et al* to be published
[31] Rolo A G, Vasilevskiy M I, Conde O and Gomes M J M 1998 *Thin Solid Films* **336** 58
[32] Morigaki K 1999 *Physics of Amorphous Semiconductors* (Singapore: World Scientific) pp 33–50
[33] Taylor D W 1988 *Optical Properties of Mixed Crystals* ed R J Elliott (Amsterdam: North-Holland) p 35
[34] Vasilevskiy M I, Baranova O V and Stroganova S V 1996 *Comput. Phys. Commun.* **97** 199